Supporting information for: On the Impact of Geometrical Factors on Hot Electron-Induced Tautomerization

Jens Kügel,[*,†] Tim Zenger,[†] Markus Leisegang,[†] and Matthias Bode[†,‡]

†*Physikalisches Institut, Experimentelle Physik II, Universität Würzburg, Am Hubland, 97074 Würzburg, Germany*

‡*Wilhelm Conrad Röntgen-Center for Complex Material Systems (RCCM), Universität Würzburg, Am Hubland, D-97074 Würzburg, Germany*

E-mail: jens.kuegel@physik.uni-wuerzburg.de;

Comparison of $\mathrm{d}I/\mathrm{d}U$ signal and electron yield

In Fig. 2(b) of the main text, it was demonstrated that the electron yield of MONA measurements can vary strongly between different data sets. These measurements were performed on defect-free areas of the Ag(111) surface with the same distance between injection point and center of the molecule. Consequently, the differences in electron yield are certainly not caused by the environment. However, we modified the tip apex between measuring the different data sets by pulsing or dipping the tip into the substrate. To analyze whether these differences of the tip apex may be responsible for the observed changes in electron yield, we performed MONA measurements on the very same HNc molecule but with different tip apexes, which were changed by gently dipping the tip into the Ag(111) surface. In Fig. S1(a) the topography of this HNc molecule is shown. Similar to all of the other measurements, the molecule was moved to a defect free area and one central proton was removed by a voltage pulse prior to this topographic scan (not shown). To characterize the tips, point spectroscopy curves of the Ag(111) surface were taken at the position of the white cross in Fig. S1(a). The resulting spectroscopy curves for three different tip apexes are presented in Fig. S1(b). Irre-

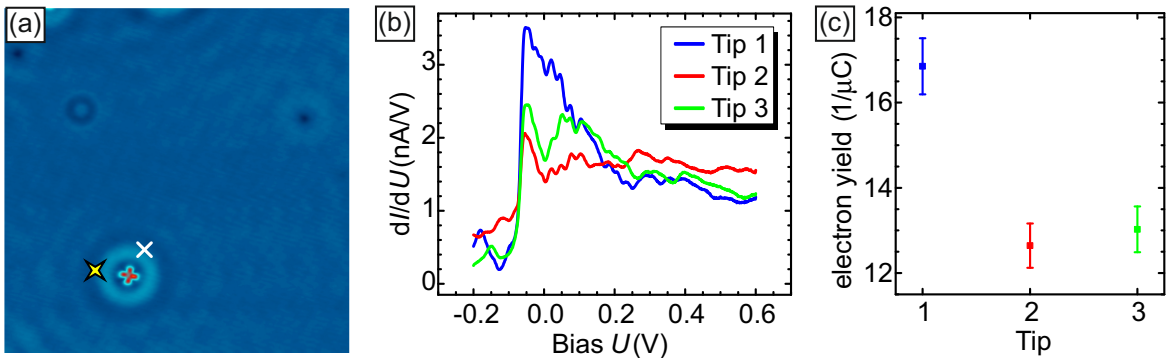

Figure S1: (a) Topography of a HNc molecule (scan paramters: $U = -50\,\mathrm{mV}$; $I = 100\,\mathrm{pA}$). (b) Spectroscopy of the Ag(111) surface taken at the white cross in (a) with three different tip apexes (spectroscopy parameters: $U_{\mathrm{set}} = 0.6\,\mathrm{V}$; $I_{\mathrm{set}} = 1\,\mathrm{nA}$; $U_{\mathrm{mod}} = 5\,\mathrm{mV}$). The tip apex was changed by very gently dipping it into the Ag(111) surface. (c) Electron yield extracted from MONA measurements with the injection point marked by the yellow cross in (a) (MONA parameters: $U_{\mathrm{exc}} = 0.5\,\mathrm{V}$; $I_{\mathrm{exc}} = 7.5\,\mathrm{nA}$; $t_{\mathrm{exc}} = 1\,\mathrm{s}$). Data points correspond to three different tip apexes, the spectroscopy curve of which are presented in (b).

spective of the particular tip apex, all spectra clearly show a step-like increase of the $\mathrm{d}I/\mathrm{d}U$ signal characteristic for the energetic onset of the electron-like surface state of Ag(111) at $E_{\mathrm{onset}} = eU_{\mathrm{onset}} \approx -63\,\mathrm{meV}$. However, the step height $\Delta\,(\mathrm{dI/dU})$ differs significantly between the three tips $[\Delta\,(\mathrm{dI/dU})_{\mathrm{Tip\,1}} > \Delta\,(\mathrm{dI/dU})_{\mathrm{Tip\,3}} > \Delta\,(\mathrm{dI/dU})_{\mathrm{Tip\,2}}]$. This trend matches the trend of the electron yield in Fig. S1(c), which was acquired by MONA measurements with exactly the same three tip apexes used in Fig. S1(b), whereby the injection point is marked by a yellow cross in Fig. S1(a).

This correlation can be explained as follows: A higher increase of the differential conductance at the onset of the surface state indicates that such a tip is more sensitive to the surface state and thus a higher fraction of electrons will tunnel into the surface state rather than into bulk states. This leads to an enhanced electron yield as hot electrons which are confined in the surface have a higher probability to reach the molecule ($\propto d^{-1}$) as compared to electrons which are injected into bulk states ($\propto d^{-2}$). Even though the analysis of the onset of the surface state reflects the overall trend of the electron yield, it cannot fully explain the differences between tip 2 and 3. Although they show a different $\Delta\,(\mathrm{dI/dU})$ their electron yield is identical within the error bar. We speculate that this ostensible contradiction is caused by the fact that we compare processes at very different energy. Namely, the step height $\Delta\,(\mathrm{dI/dU})$ is determined at the onset of the Ag(111) surface state, i.e., $E_{\mathrm{onset}} \approx -63\,\mathrm{meV}$ In contrast, the tautomerization of the molecule is triggered by hot electrons with an energy that exceeds the threshold of the N-H–stretching mode ($eU \approx 407\,\mathrm{meV}$). The MONA measurements were always performed with an excitation voltage of $U_{\mathrm{exc}} = 0.5\,\mathrm{V}$, i.e., the dominant contribution will come from electrons in the energy range $407\,\mathrm{meV} \leq E_{\mathrm{hot}} \leq 500\,\mathrm{meV}$. Indeed, careful inspection of spectra 2 and 3 in Fig. S1(b) reveals that the $\mathrm{d}I/\mathrm{d}U$ signal inverts at $U \approx 0.2\,\mathrm{V}$, i.e., right between the energy ranges relevant for the surface state onset and molecule tautomerization.

Calculations of the residence times

In Fig. 2(d) of the main text the normalized residence time is presented. In the following the different steps performed to calculate this data set will be described. In Fig. S2(a) the probability is shown that a proton bound to a metastable arm is detected at the same metastable arm after the next excitation pulse. We have to realize, however, that due to the relatively short lifetime of the metastable state this probability is not equivalent to the probability that the proton remained at the metastable arm in the meantime. It is also possible that the proton switched to a stable arm and was again excited to the same metastable arm by the excitation pulse. Unfortunately, it is not directly possible to distinguish these two cases as the initial and the final state in both processes is the same. To circumvent this issue, we made use of the fact that the probability of exciting the proton from a stable arm to a metastable is—within statistical error—the same as the excitation to the other metastable arm. Consequently, the probability that a proton switched from a metastable to a stable arm and is excited back to the same metastable arm can be approximated by the probability that a proton switched from a metastable to a stable arm and was excited to the opposing metastable arm. The latter probability is shown in Fig. S2(b). This probability was subtracted from (a) to calculate the residence time, which is shown in Fig. S2(c). The same procedure was also applied to the stable states, which is presented in Fig. S2(d-f). This is necessary because a proton bound to the stable state might be excited to a metastable state and switch back to the stable state before the state of the molecule is probed. In Fig. S2(g) and (h) we plot the residence time of the metastable (c) and stable (f) state after normalization to the 0°-direction. The average value of these normalized data sets corresponds to the plot shown in the main text, which is also shown in Fig. S2(i).

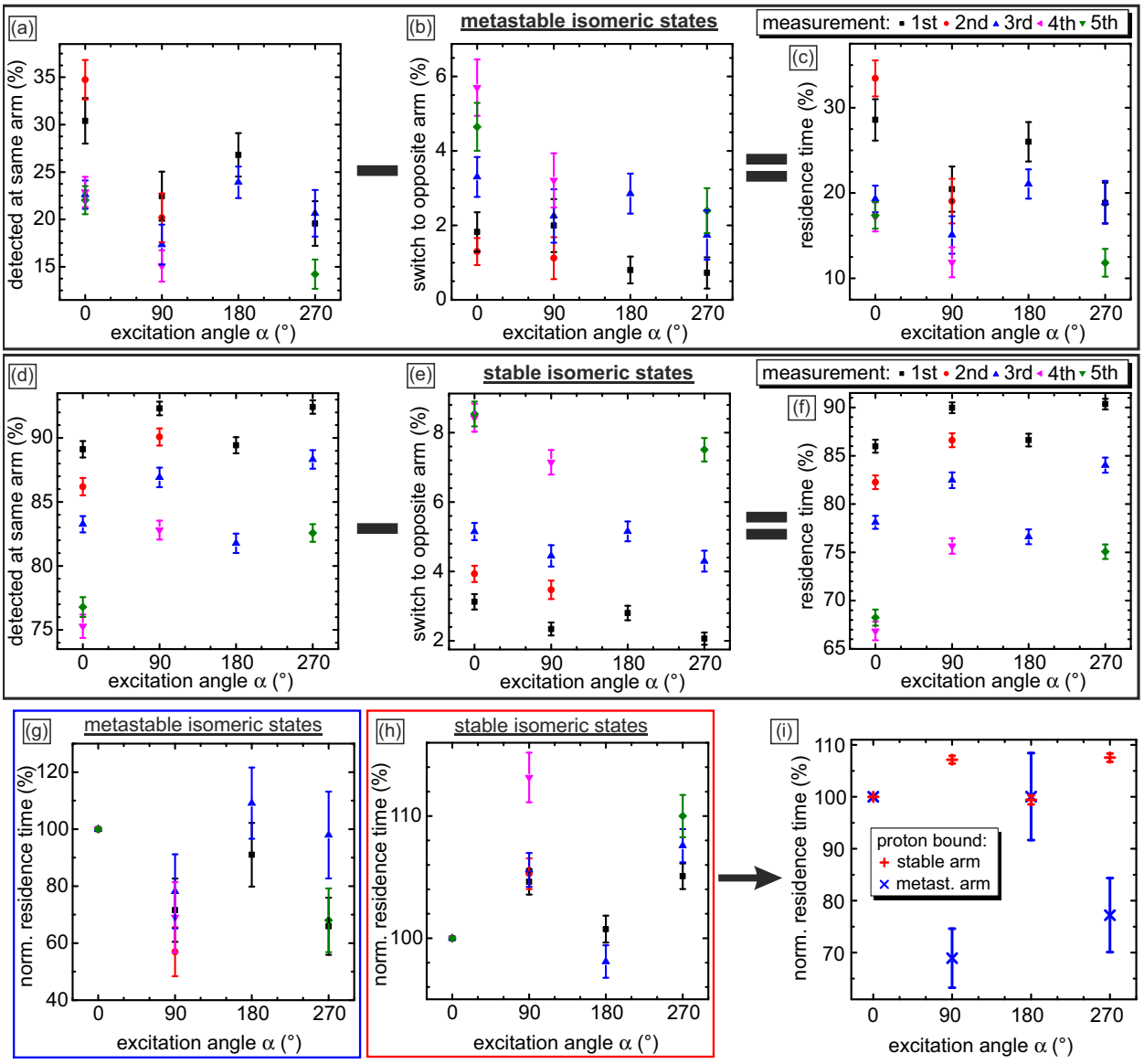

Figure S2: (a) Probability that a proton bound to a metastable arm is detected at the same arm after the next excitation pulse. The five data sets correspond to the measurement of Fig. 2 in the main text. (b) Probability that a proton bound to the metastable arm is detected at the opposing arm after the next excitation pulse. (c) Residence time of the metastable state, which was calculated by subtracting (b) from (a). (d) Probability that a proton bound to a stable arm is detected at the same arm after the next excitation pulse. (e) Probability that a proton bound to the metastable arm is detected at the opposing arm after the next excitation pulse. (f) Residence time of the stable state, which was calculated by subtracting (e) from (d). (g)/(h) Residence time of the metastable/stable state (c)/(f), normalized to the data points of the 0°-direction. (i) Average value of the normalized residence time

Details on the fit function

The angle- and distance-dependent MONA measurements of deprotonated phthalocyanine and naphthalocyanine molecules were presented in Fig. 4(b) and Fig. 5(d) of the main text, respectively. Both data sets were fitted with a simple geometrical analysis, which is shown in Fig. S3 for the three injection angles 0°, 90°, and 45°. The molecular arms (blue and red rectangles) are approximated by rectangularly shaped boxes with length a and width w. Within our model the stable arm (blue) and metastable arm (red) possess different efficiencies, P_{stab} and P_{metastab}, to convert the energy of hot electrons into switching events. Phase coherence length is neglected. For simplicity it is assumed that every hot electron reaching a molecular arm will be adsorbed and that the propagation of the hot electrons is confined within the surface. With these assumptions, the distance-dependent electron yield $P(d)$ can be calculated by multiplying the converting efficiency P_{stab} and P_{metastab} with the

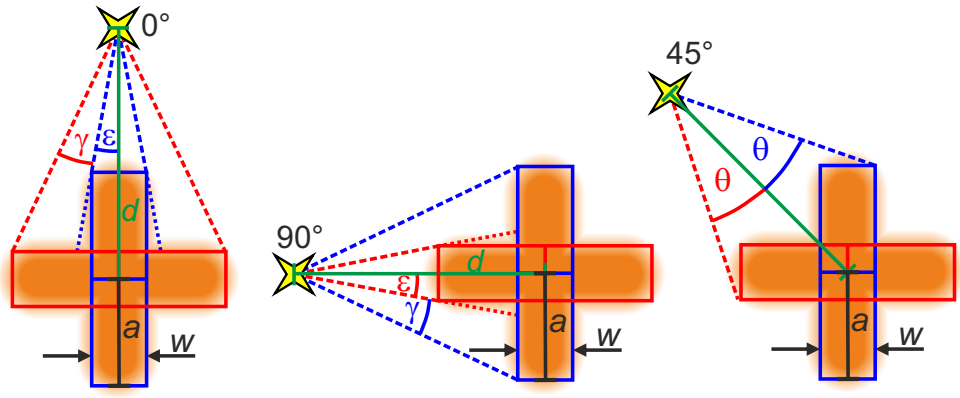

Figure S3: Geometrical model of phthalocyanine and naphthalocyanine molecules used to fit the distance- and angle-dependent MONA data sets. The molecules are approximated by rectangular shaped arms (blue and red), whereby the stable arms (blue) and metastable arms (red) are characterized by different efficiencies to convert hot electrons into switching events.

Table S1: Fit-parameters for the distance- and angle-dependent measurements of a singly deprotonated phthalocyanine (HPc) and napthalocyanine (NPc) molecule

Parameter	HPc-fit	HNc-fit
P_{stab}	$(60.4 \pm 71.8)/(\mu\mathrm{C})$	$(109 \pm 165)/(\mu\mathrm{C})$
P_{metastab}	$(12.5 \pm 21.3)/(\mu\mathrm{C})$	$(29.1 \pm 34.6)/(\mu\mathrm{C})$
$P^*_{\mathrm{metastab}} + P^*_{\mathrm{stab}}$	$(68.3 \pm 53.1)/(\mu\mathrm{C})$	$(127 \pm 119)/(\mu\mathrm{C})$
a	$(0.367 \pm 0.267)\,\mathrm{nm}$	$(0.615 \pm 0.583)\,\mathrm{nm}$
w	$(0.412 \pm 0.346)\,\mathrm{nm}$	$(0.478 \pm 0.276)\,\mathrm{nm}$

associate angle γ, ϵ or θ:

$$\begin{aligned} P_{0^\circ}(d) &= P_{\mathrm{stab}} \cdot 2\epsilon + P_{\mathrm{metastab}} \cdot 2\gamma \\ &= P_{\mathrm{stab}} \cdot 2 \cdot \mathrm{ArcTan}\left(\frac{w/2}{d-a}\right) + P_{\mathrm{metastab}} \cdot 2\left(\mathrm{ArcTan}\left(\frac{a}{d-w/2}\right) - \mathrm{ArcTan}\left(\frac{w/2}{d-a}\right)\right) \end{aligned}$$

$$\begin{aligned} P_{90^\circ}(d) &= P_{\mathrm{metastab}} \cdot 2\epsilon + P_{\mathrm{stab}} \cdot 2\gamma \\ &= P_{\mathrm{metastab}} \cdot 2 \cdot \mathrm{ArcTan}\left(\frac{w/2}{d-a}\right) + P_{\mathrm{stab}} \cdot 2\left(\mathrm{ArcTan}\left(\frac{a}{d-w/2}\right) - \mathrm{ArcTan}\left(\frac{w/2}{d-a}\right)\right) \end{aligned}$$

$$\begin{aligned} P_{45^\circ}(d) &= P^*_{\mathrm{metastab}} \cdot \theta + P^*_{\mathrm{stab}} \cdot \theta \\ &= (P^*_{\mathrm{metastab}} + P^*_{\mathrm{stab}}) \cdot \mathrm{ArcTan}\left(\frac{a + w/2}{\sqrt{2} \cdot d + w/2 - a}\right) \end{aligned}$$

The results of these functions for the phthalocyanine and napthalocyanine molecule are listed in Tab. S1.